Geol Rundsch (1995) 84:137–150

ORIGINAL PAPER

B. J. Haupt · C. Schäfer-Neth · K. Stattegger

Three-dimensional numerical modeling of Late Quaternary paleoceanography and sedimentation in the northern North Atlantic

Received: 12 April 1994 / Accepted: 10 August 1994

Abstract Modelling of Late Quaternary paleoceanography and sedimentation in the northern North Atlantic (NNA) is achieved by coupling the ocean general circulation model SCINNA (Sensitivity and Circulation In the NNA) to the sedimentation models SENNA (SEdimentation In the NNA) and PATRINNA (PArticle TRacing In the NNA).

SCINNA is based on the primitive equations with conservation of mass, momentum, energy, heat and salt. SENNA and PATRINNA are driven by temperature, salinity and velocity fields derived from SCINNA. The modelling includes three-dimensional circulation of the ocean, sediment transport in the water column and two-dimensional sedimentary processes in a thin bottom layer. SENNA calculates the erosion, transport and deposition of sediments, resulting in sedimentation patterns for specific time intervals. PATRINNA models the transport paths of single sediment grains corresponding to the ocean circulation.

The NNA reacts in a highly sensitive manner to small forcing changes, as shown by our sensitivity experiments. From these experiments it is possible to model specific circulation regimes for glacial and interglacial periods, for melt water events and for the onset of glaciation. The different climatic stages in the circulation model produce different sediment patterns in the sedimentation models, which correspond closely to the sedimentary record.

Key words Numerical modeling · Paleoceanography Sedimentation · Sediment transport · North Atlantic Greenland-Norwegian Sea

Bernd J. Haupt (✉) · Christian Schäfer-Neth · Karl Stattegger
Geologisch-Paläontologisches Institut und Sonder-Forschungs-Bereich 313, Universität Kiel, Olsenhausenstrasse 40–60, D-24118 Kiel, Germany

Introduction

The northern North Atlantic (NNA) is an ocean area highly sensitive to climatic changes. Its specific thermohaline circulation system, driven by surface heat and freshwater fluxes, ice cover and wind, is not stable in time and strongly affects global ocean climatology and sedimentation (Broecker and Peng 1982; McCave and Tucholke 1986; Sarnthein et al. 1994).

The sedimentary record of the NNA for the Late Quaternary is based on more than 100 deep sea cores. A high resolution isotope stratigraphy was developed from these cores. In addition, the cores provide data on sedimentation rates and much proxy data about paleotemperatures, paleo-salinities and paleo-productivity for various basin-wide time slices, which correspond to short synoptic climatic intervals (CLIMAP 1981; Duplessy et al. 1991; Pflaumann et al. submitted; Sarnthein et al. (1994) issue). This paleoceanographic data led to different interpretations and occasionally contradictary concepts of the NNA's climatic history.

Numerical modeling provides valuable tools to overcome these problems. Ocean general circulation models (OGCMs) based on ocean physics calculate typical circulation patterns from climate-specific model forcing for different time slices. Sensitivity experiments are used to test the consistency of physical parameters deduced from the proxy data. Sedimentation models calculate the fill of sedimentary basins using sediment physics and hydrodynamics. Their power increases tremendously by coupling with an appropriate OGCM.

Only a few OGCMs exist for the NNA which extend beyond 65 N latitude. The models of Legutke (1991) and Stevens (1991) cover the Greenland–Iceland–Norwegian Seas and the NNA from 57.5 N to 82.5 N, respectively, with open boundaries to the adjacent areas. As shown by these workers, the model's state depends critically on the positions of the flows across the margins, as well as their mass, heat and salt transport. For past time slices, transport estimates from proxy data do not exist and open boundaries cannot be used for our

studies. Instead, the boundaries are kept closed. Initially, this appears even more unrealistic, but placing the closed walls far away from the area of interest minimizes any unrealistic features. Furthermore, the use of restoring zones along the closed walls reintroduces the world ocean's water mass transformation. Within these zones, the temperatures and salinities are forced to prescribed values with some given time constant. Thus, for example, cold deep water entering the restoring area at the southern closed margin will be upwelled and with leave it as warm surface water moving northwards. As paleo-reconstructions of temperatures and salinities *are* available, these can be used for restoring purposes when modelling the paleo-circulation. Therefore, the closed boundary/restoring approach is well suitable for paleo-modeling. Such an approach is also used by Aukrust and Oberhuber (in press) in their model of the modern Atlantic, which is driven by surface heat and freshwater fluxes. However, surface flux data have not been reconstructed for past times. An intermediate numerical model was used by Seidov et al. (submitted) in combination with proxy data to investigate three major states of the ocean circulation: modern state, melt water event (13.6 ka BP) and last glacial maximum (18 ka BP). This model is based on the geostrophic relation and a coarse resolution grid.

Several sedimentation models have been developed during the last few years to simulate the filling history of sedimentary basins. Many of these models are two dimensional and display the sediment fill in vertical cross-sections which correspond to synthetic seismograms. Model calculations use data on basin geometry, subsidence, sea-level changes and sediment supply. Depending on the model physics, sediment transport, deposition, erosion, compaction and the resulting sediment body can be simulated (Kendall et al. 1991; Syvitzki and Daughney 1992). Process oriented dynamic two- and three-dimensional models are driven by flows and their transport velocities in the transport medium. These flows carry sediment particles of various grain sizes and are used to calculate erosion, transport and sedimentation (Bitzer and Pflug 1989; Tetzlaff and Harbaugh 1989; Lee and Harbaugh 1992). Models of this type are efficient in modelling sedimentation in small basins where sediment is supplied from punctual lateral sources, e.g. deltaic sedimentation. However, the modeling of large basins needs an extremely high computing capacity and is very time consuming. The coupling of dynamic sedimentation models to relatively simple OGCMs has so far been successfully performed only in shallow marginal seas (Erickson et al. 1989; Sündermann and Klöcker 1983).

This study of the Late Quaternary paleoceanography and sedimentation in the NNA aims to: (1) realistically simulate the modern NNA circulation; (2) couple a suitable sedimentation model to the OGCM; (3) validate the simulated modern sedimentation patterns with the observed patterns; (4) trace individual sediment particles through space and time; and (5) simulate different ocean circulation modes and the resulting sedimentation patterns corresponding to the paleoceanographic record. Existing models do not fulfill all these aims. Therefore, the new modeling approach presented here was developed.

Models and model area

Considering the modelling goals and the specific regional setting outlined above, three numerical models were developed: (1) SCINNA, Sensitivity and CIrculation in the NNA; (2) SENNA, SEdimentation in the NNA; and (3) PATRINNA, PArticle TRacing In the NNA.

These models are coupled in the following way: firstly, SCINNA calculates the oceanic circulation; the modelled circulation then initializes SENNA and PATRINNA to simulate the sedimentary system.

In general, an inverse procedure is used. The solutions of the forward models optimize the matching of predictions and existing data. SCINNA uses data based temperature, salinity, ice and wind speed distributions to calculate the oceanic circulation. SENNA and PATRINNA use the model circulation to calculate the erosion, transport and deposition of sediments. The models run multiple times, each time comparing model predictions with the data and adjusting the models progressively if the quality of the data is high compared with the sensitivity of the models. Measured data and proxy data constrain the models' solutions. However, the errors present in the data increase the confidence limits of the model results. Conversely, the physically consistent models indicate possible inconsistencies in the data and their confidence limits. The influence and validity of single parameters and variables on the modelled system can successfully be proved by sensitivity experiments.

Model area

SCINNA, SENNA and PATRINNA use the same grid and topography, covering the NNA, the Norwegian–Greenland Sea, the Barents Sea and parts of the Polar Basin. The coordinate system is spherical, where the equator has been rotated up to 60°N along zero meridian. In this way, the convergence of meridians is minimized. Conventional geographical coordinates would yield a very narrow grid spacing in the model's northern regions and in turn require very short time steps. With this rotation, a horizontal resolution of 0.5° and 95 grid points in both directions, the spacing is about 50 km everywhere and a time step of 12 hours can be used. The vertical is split into 17 levels, so that topography can be represented in a realistic manner (Fig. 1) [level, depth (m)]: 1, 50; 2, 100; 3, 150; 4, 200; 5, 300; 6, 400; 7, 500; 8, 750; 9, 1000; 10, 1250; 11, 1500; 12, 2000; 13, 2500; 14, 3000; 15, 3500; 16, 4000; and 17, 5000.

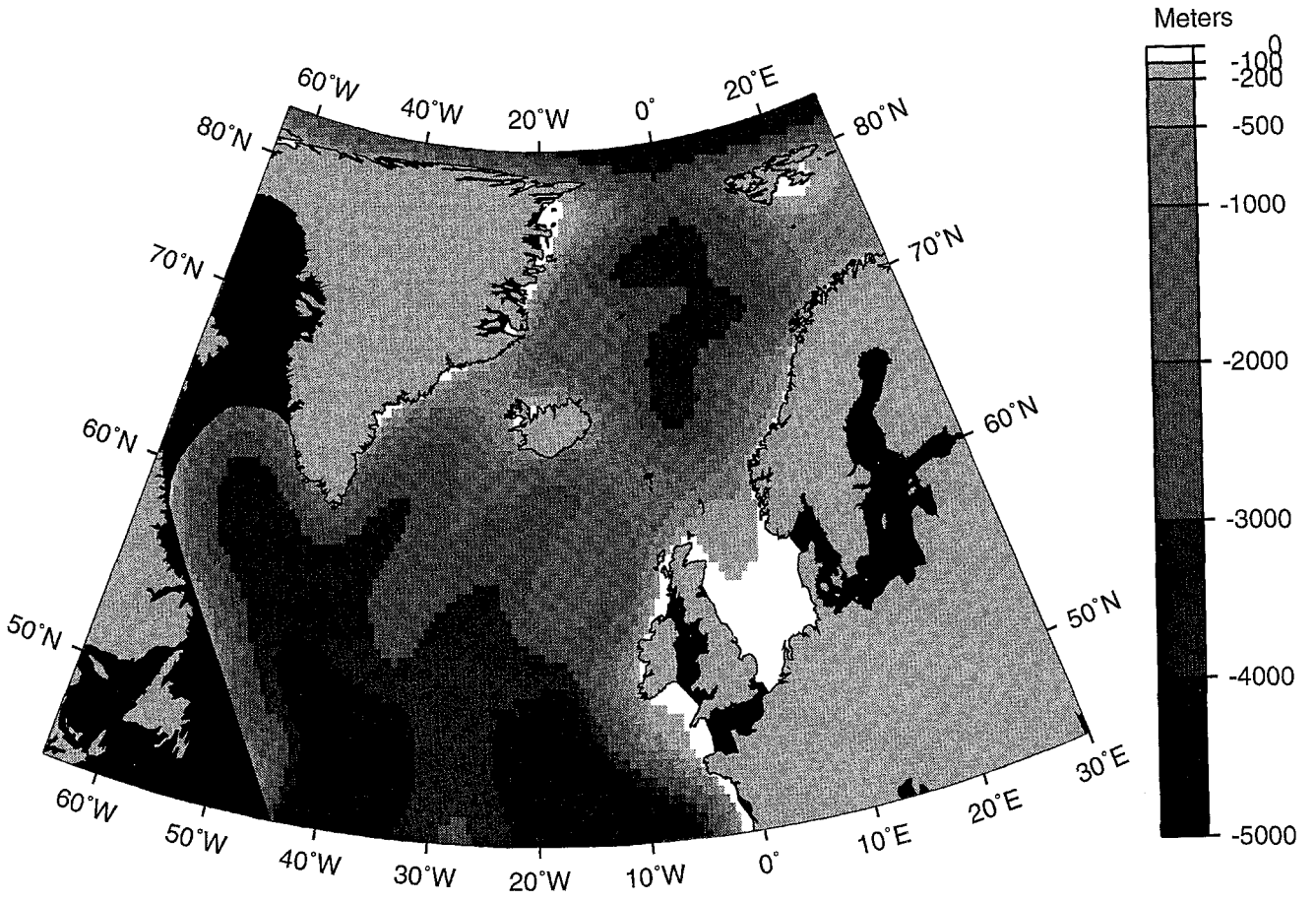

Fig. 1 Modern model topography

SCINNA

In principle, the state of the Norwegian–Greenland Sea cannot successfully be modeled without taking into account the influence of the complete world ocean, especially its transformation of water masses. However, limited computer resources restrict the resolution of global models. Consequently, SCINNA covers only a very small part of the world ocean, with closed boundaries and restoring zones where the other parts of the ocean have been clipped off.

To facilitate the work with different data sets and time slices, SCINNA allows the employment of: (1) arbitrarily shaped basins, taking into account topographic variations due to sea level changes and glaciation/deglaciation processes; (2) any temperature and salinity initialization fields; (3) arbitrary temperature, salinity ice and wind distributions for forcing the model; (4) arbitrary temperature and salinity restoring data; and (5) a simple thermodynamic prognostic sea ice model instead of a fixed ice cover.

SCINNA is a three-dimensional prognostic OGCM. It has been developed on the basis of the modular ocean model (Pacanowski et al. 1991), the newly built version of the well known Princeton circulation model (Bryan 1969; Cox 1984).

Being appropriate for modeling motions on a rotating sphere, SCINNA is written in three-dimensional spherical coordinates (refer to the appendix for an explanation of symbols and definitions). It uses the set of primitive equations, comprising conservation of momentum, mass, heat and salt (Fig. 2). A non-linear equation of state is used.

At the lateral boundaries the no-slip condition (the fluid adheres to the walls) and no-flux conditions (no heat and salt fluxes across the walls) are applied, the surface boundary conditions take into account the momentum transfer by winds and the fluxes of heat and freshwater. For eliminating external gravity waves – which require very short time steps and very long computing time – the rigid-lid condition (no sea surface elevation) is used. At the bottom the momentum flux is given by bottom friction and the tracer fluxes are kept at zero, as is the case for the lateral boundaries. The boundary condition for vertical velocity ensures that the fluid is forced to follow the bottom slopes.

For discretization the Arakawa-B grid (Mesinger and Arakawa 1976) is used, with a shift of a half-grid distance between T–S points and u–v points (Fig. 3a). For integration in time the leap-frog scheme is used, calculating the model's new state at a given time step n from the state of two time steps earlier $(n-2)$ and the time derivates of the previous time step $(n-1)$ (Fig. 3b).

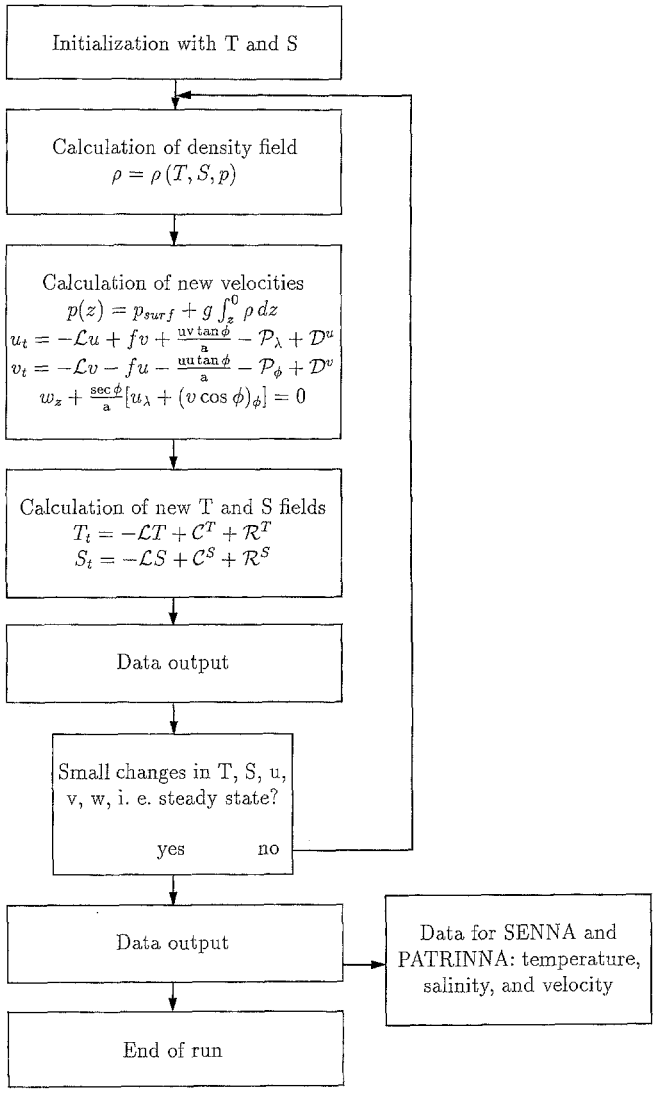

Fig. 2 Integration scheme of SCINNA; see Appendix for explanation of symbols

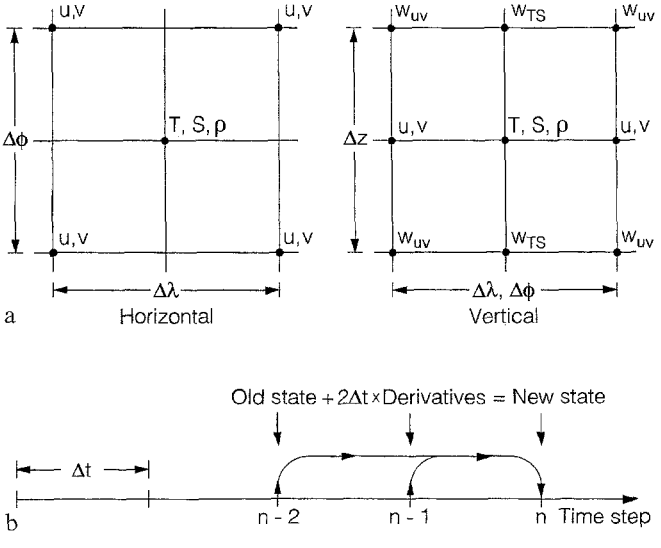

Fig. 3 **a** Model grid; **b** time discretization

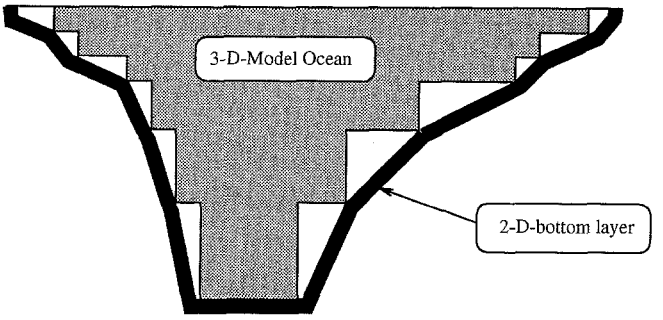

Fig. 4 Two- and three-dimensional components in SENNA and PATRINNA

SENNA

SENNA is a large-scale dynamic three-dimensional sedimentation model for the NNA. It basically consists of two coupled models, the first modeling the three-dimensional sediment transport in the water column, the second simulating the two-dimensional processes near the bottom in a layer 1 cm thick. These two models are coupled by the vertical exchange of suspended sediment (Fig. 4). SENNA is driven by temperature, salinity and velocity fields derived from experiments with ocean circulation models such as SCINNA.

Although the bottom topography is represented as a structure of stairs in the three-dimensional model, this can be neglected in the two-dimensional bottom layer, which is kept parallel to the newly computed bottom shape at any time. In this way, a realistic modeling of processes parallel to the bottom slopes is possible. A detachment of the flow from the stairs of the bottom topography in the three-dimensional model is only possible with turbulence where the angle of the bottom slope exceeds 5° (Puls 1981). This bottom slope in the flow direction is not reached in the model (maximum $\leqslant 2.65°$).

The structure of the model physics is simple so as to be able to run long-time simulations (Fig. 5). It is possible to model sediment dynamics based on terrigenous and biogenic sediment entry within a reasonable computer time. At the same time it is important to be able to resuspend and redeposit sediments that have already been deposited. The three-dimensional model essentially contains a three-dimensional sediment transport equation, and the two-dimensional model is based on a two-dimensional sediment transport equation. The lateral boundaries are closed as for SCINNA. In the three-dimensional model the lateral entry of sediments and the entry of particles, which come from melting icebergs into the upper part of water column, are taken into account. At the lateral and surface boundaries positive sediment sources for sediment entry and negative sediment sources for sediment sinks are prescribed at the boundaries. The mass of sediments can thus be reduced or increased within the model. These changes of the total mass of sediment in the water column are also

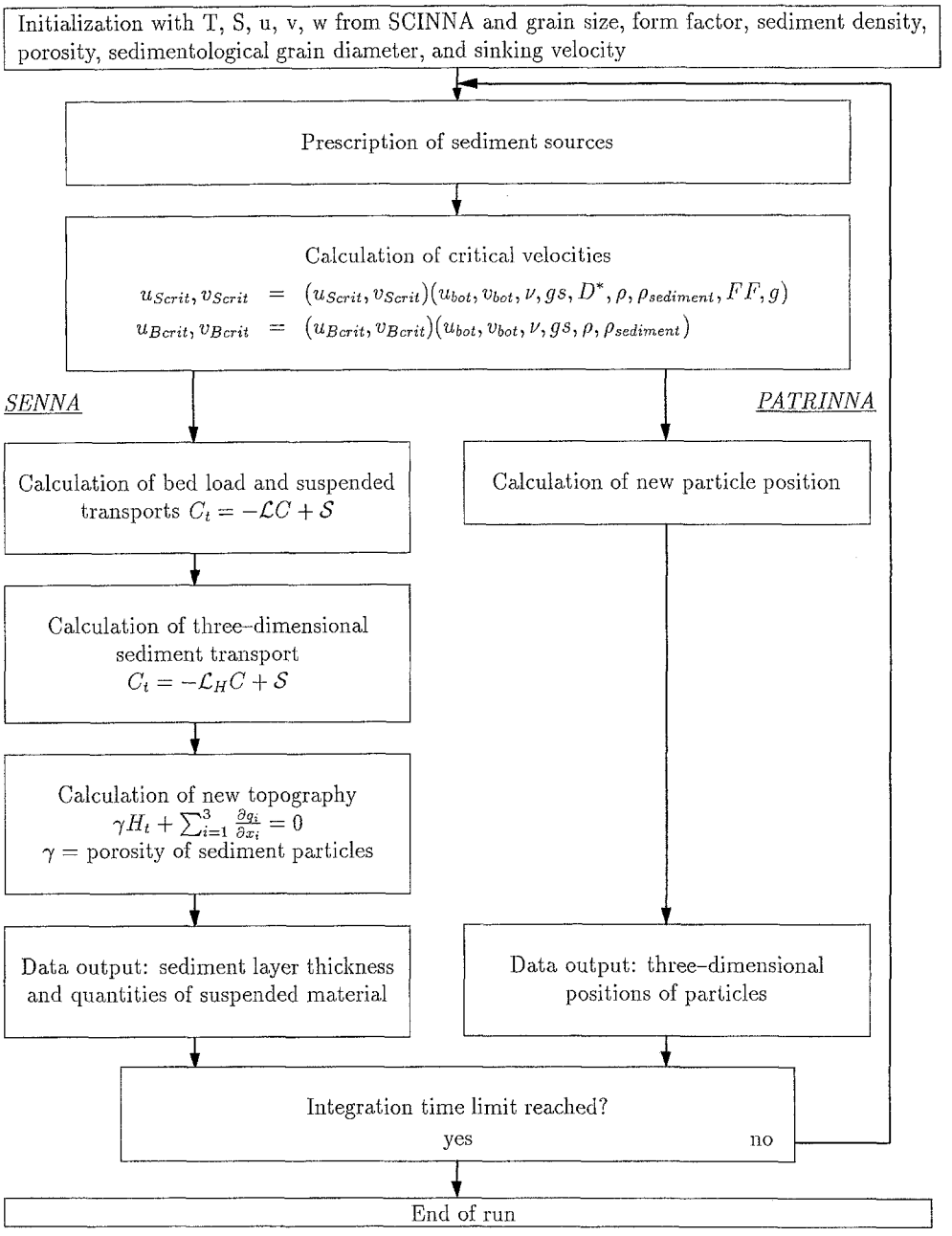

Fig. 5 Integration schemes of SENNA and PATRINNA; see Appendix for explanation of symbols page 150

envoked by erosion, redistribution and deposition. The particles that are suspended in the water column are carried by the currents (Bitzer and Pflug 1989). In addition to the vertical velocity of the surrounding water, the sink velocity of particles has to be considered. This velocity depends on the grain size, density and kinematic viscosity of the surrounding water as well as on particle density, form factor and sedimentological grain diameter (McCave and Gross 1991; Zanke 1977).

In the two-dimensional bottom model, near-bottom processes are considered. These include erosion, transport and deposition, which depend on critical velocities – i.e. critical erosion and suspension velocity – and on the sediment contents of the 1 cm thick bottom layer, as well as grain size and form factor (McCave 1984; Zanke 1977, 1978). The near-bottom velocities result from a reduction in the velocity of the three-dimensional models' layer most proximal to the bottom (Sündermann and Klöcker 1983; Zanke 1978). Also, the bottom slope in the *direction* of the bed load and the suspension load transport (Krohn 1975; Puls 1981) is taken into account. An upward directed bottom slope increases the critical velocities and at the same time reduces the erosion rate, and vice versa. The change in the bottom topography is calculated from the modeled changes of the sediment contents in the 1 cm thick bottom layer (Puls 1981; Sündermann and Klöcker 1983).

To simplify calculations, the combined models are based on a homogeneous grain mixture with constant sink velocity (0.05 cm s^{-1}) (Sündermann and Klöcker 1983). In this instance the grain size can be neglected. As elementary relations of sediment movements usual-

ly depend on mechanical processes, and because of the mostly unknown influence of biological factors on waters, the following effects are not considered: (1) coagulation by micro-organisms; (2) the roughness of sediment changes due to organic films; (3) the flocculation effects of organic sediments and mixtures with sands; and (4) cohesion. The motion of the sea in the upper layers is also neglected.

PATRINNA

PATRINNA consists, as SENNA, of two coupled models. The three-dimensional model calculates the three-dimensional drift in the water column. The two-dimensional model considers the drift parallel to the seafloor. Both models were developed for tracing particles. With PATRINNA the main drifting patterns can be worked out as well as the residence time of the particles or sediment plumes/clouds in different areas or basins, respectively.

PATRINNA uses the same driving fields as SENNA, together with the topography changes computed by the latter (Fig. 5). As in SENNA, particles are considered to move horizontally with the prescibed horizontal velocity (Bitzer and Pflug 1989). The vertical velocity is calculated by the continuity equation from SCINNA's horizontal velocities. The sink velocity of particles is superimposed. This velocity originates from observations and from empirical equations (Zanke 1977; Gibbs 1985). PATRINNA uses the reduced bottom velocity of SENNA in the bottom layer (Sündermann and Klöcker 1983; Zanke 1978).

The bottom slope is considered in the same way as in SENNA. The development of the bottom topography within time is not taken into consideration because changes are insignificant and can thus be neglected due to the relatively short PATRINNA runs (less than 50 years). Special attention is given to the reconnaissance of the mean sediment drifts and to the residence time of particles and particle clouds in different regions.

Interconnection and coupling of the models

SCINNA is initialized with temperatures and salinities from measurements and/or paleo-reconstructions. With the application of surface wind, temperature, ice and salinity distributions, time integration proceeds until the rate of change of the model's state is small compared with the rates indicated by proxy data (Fig. 2). At this point, the temperatures, salinities and velocities are transferred as initial fields to SENNA and PATRINNA and kept constant in time. These models in turn calculate the sedimentation processes for the desired time interval (Fig. 5).

Because the topographic changes due to sedimentation/erosion processes are negligible compared with SCINNA's vertical resolution, a coupling from SENNA back to SCINNA is not necessary.

Results and discussion

Here the results of two experiments will be discussed, the first (M) was run to model the modern situation; the second (LGM) gives the first results for the last glacial maximum (18000 ^{14}C years, 21500 calendar years BP).

Experiment M used the topography shown in Fig. 1 and was initialized with the winter temperatures and salinities of Levitus (1982) and Dietrich (1969). These data sets were also used for restoring and thermohaline forcing (Fig. 6). For thermal forcing, the original temperatures were replaced by $-1.90°$ C below the typical winter ice cover (Fig. 6a). The wind stress was taken from the January data of Hellerman and Rosenstein (1983).

To account for glacial sea-level change, the overall depth was reduced by 100 m in the LGM experiment. Within this new topography, the glaciers laying on the shelves were simulated by removing all regions between 0 and 200 m depth from the water body (Fig. 7). With the exception of the Bear Island Trough this procedure cuts off the Barents Sea and the North Sea, and

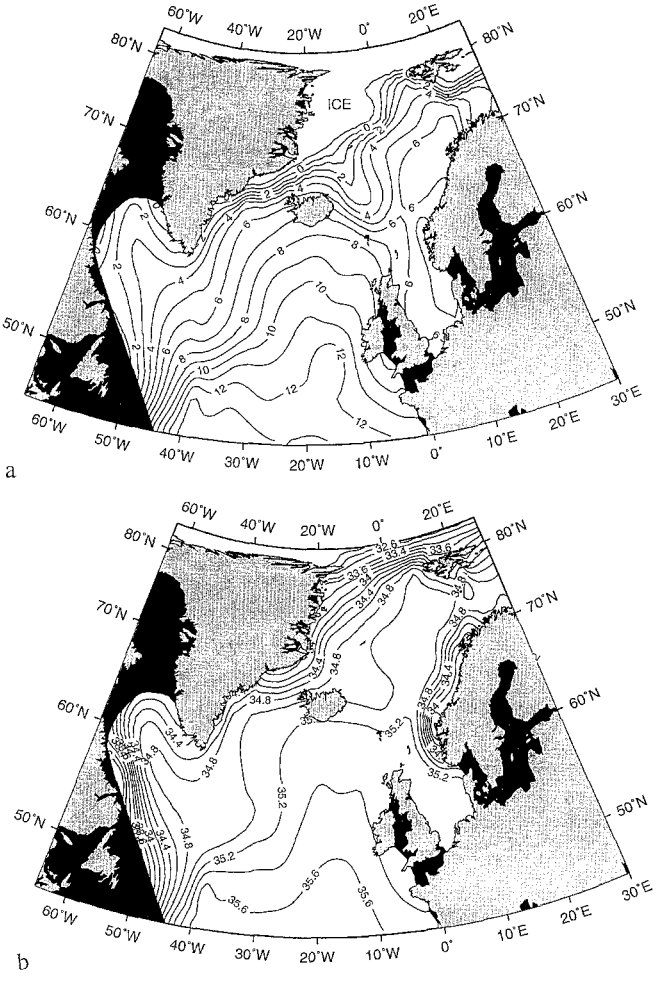

Fig. 6 **a** Modern winter sea surface temperature in °C and mean winter ice cover. **b** Modern winter sea surface salinity in ‰

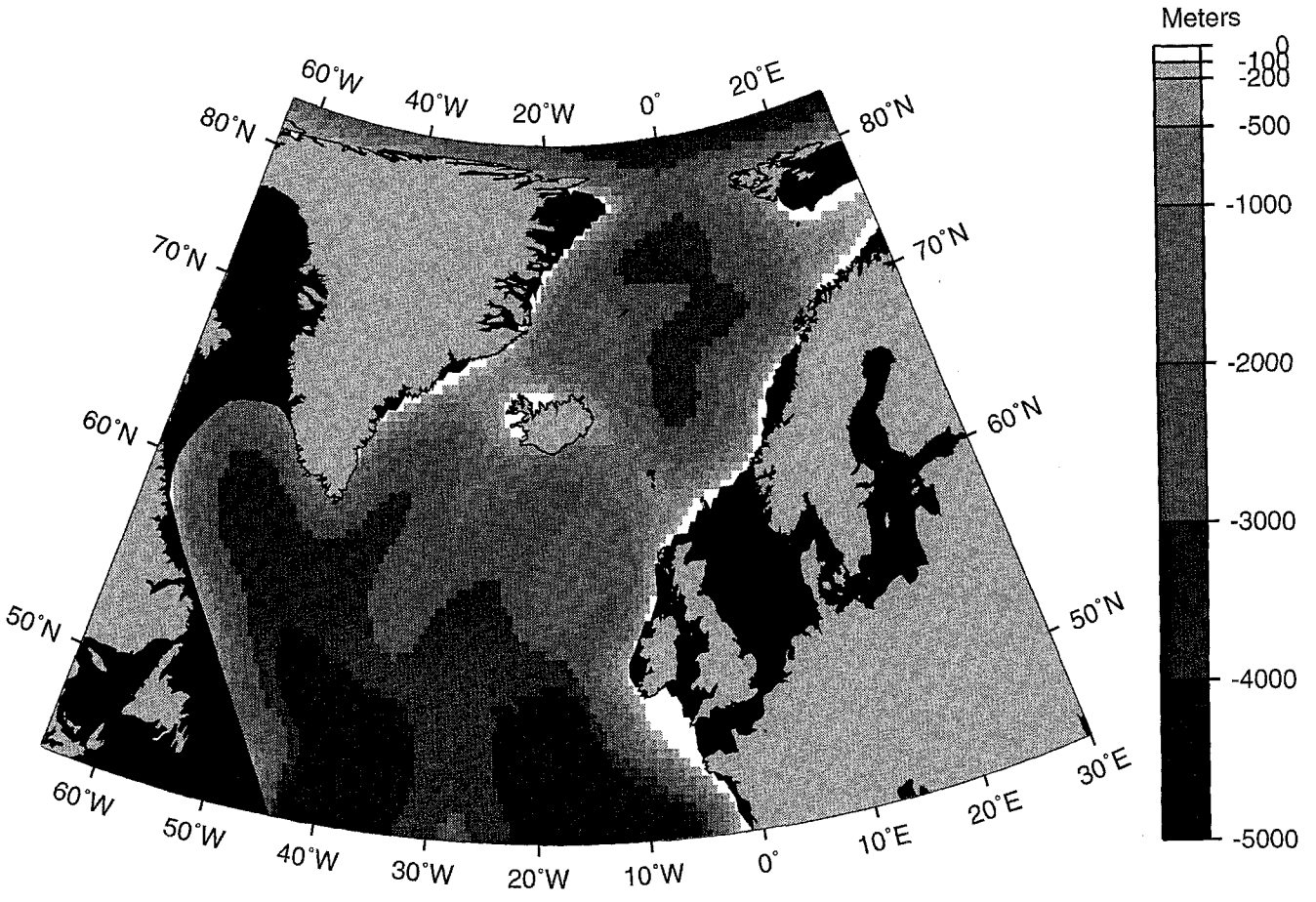

Fig. 7 Model topography for the LGM experiments

reduces the cross-sectional areas of the straits between Greenland, Iceland and Scotland. Initialization and wind forcing were identical to those of experiment M. For thermal forcing and ice cover the CLIMAP summer reconstruction was used (Fig. 8a), whereas for haline forcing a superposition of salinity reconstructions by Duplessy et al. (1991) and Sarnthein, Seidov and Weinelt (personal communication, Fig. 8b) was used. The LGM winter reconstructions were very poor, so we first tried to model the summer situation derived from the available proxy data. These surface forcing data are by no means consistent with the modern three-dimensional distributions of temperature and salinitiy, so that the latter cannot be used for restoring. However, recent three-dimensional paleo-reconstructions (Sarnthein et al. 1994) have not yet been prepared for model use, so this experiment was run without restoring.

With the modern forcing, SCINNA produces all prominent circulation patterns as they are known for today. Figure 9a shows the resulting stream function – i.e. the vertically integrated mass transport after 50 years of integration. Values are given in Sverdrups ($1\ \mathrm{Sv} = 10^6\ \mathrm{m}^3\,\mathrm{s}^{-1}$), negative for cyclonal, positive for anticyclonal motion. The subtropical and subpolar gyres are apparent, presenting a schematic Gulf Stream and Labrador Current at their respective western boundaries. The two gyres are separated by the North Atlantic Current directed north-east from Newfoundland to Ireland. Its continuation, the Norwegian Current, enters the Norwegian Sea with a transport of approximately 1.5 Sv. This inflow is balanced by the combined outflows of the East Greenland and East Iceland currents.

In the LGM experiment the absence of lateral restoring reduces the transports of the subtropical and subpolar gyres, and the Gulf Stream and the Labrador Current are notably less sharp than in the modern run. The gyres' shapes, however, remain essentially the same (Fig. 9b).

The main differences between M and LGM occur in the Greenland–Norwegian Sea and at the ridges between Greenland, Iceland and Scotland. The combination of temperatures around freezing point (Fig. 8a) and high salinity at the surface (Fig. 8b) causes an intensification of the cyclonal circulation to values of about 6 Sv in the LGM run, whereas the flows over the ridges are reduced to approximately 1 Sv because of reduced sea level.

It should be kept in mind that the reliability of the model results is subject to the quality of both the model and its input data. Firstly, the model has to be physically correct and, secondly, the input data must be consistent and appropriate for the studied phenomena. Thus,

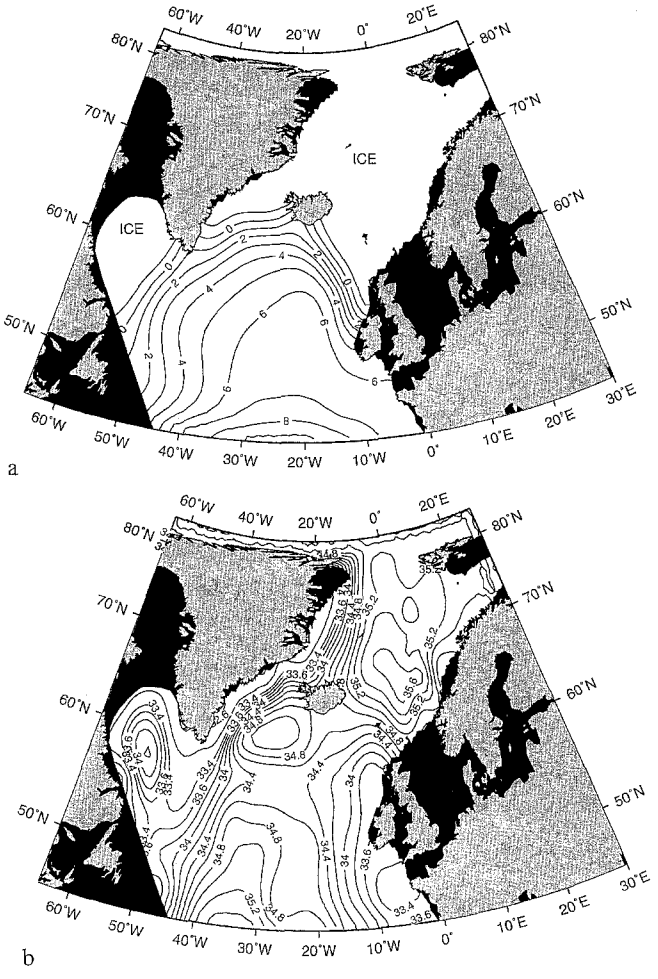

Fig. 8 **a** CLIMAP summer sea surface temperature for the LGM in ° C. **b** Summer sea surface salinity for the LGM in ‰

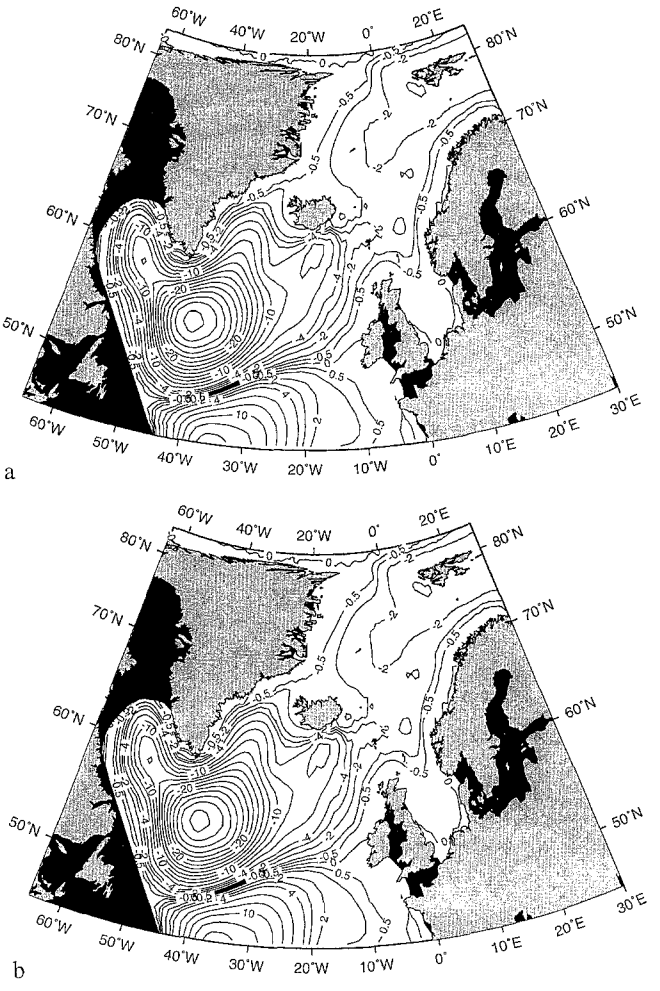

Fig. 9 **a** Modern circulation pattern, vertically integrated mass transport in Sv. **b** LGM circulation pattern, vertically integrated mass transport in Sv

numerous sensitivity experiments need to be performed before any successful modeling of a given situation. In this instance, these sensitivity tests were based on the modern state of the NNA and revealed a very high sensitivity of the model to even small changes in the forcing fields. Variations of temperature and salinity at the surface and ice-edge position within ranges comparable with their respective paleo-reconstruction error estimates can alter the modeled oceanic state significantly. This is particularly so with respect to the influences of surface salinity and ice cover.

To illustrate the latter's importance, the results of two experiments with SCINNA in normal (i.e. non-rotated) geographical coordinates will be shown here. Both model runs were initialized and driven by the annual temperature and salinity data from Levitus (1982) and the annual winds from Hellermann and Rosenstein (1983). The only difference between the runs was imposed by the ice cover, which cuts off the momentum transfer by the winds and keeps the surface temperature at freezing point. The heavy lines in Fig. 10 show the respective positions of the ice edges, together with the resulting stream functions. In experiment (a), the relatively narrow sea ice cover does not mantain the cold and dense intermediate water, causing an unrealistic anticyclonal motion (positive stream function values) in the Greenland Sea. In experiment (b), a small shift of the ice edge to the south-east yields a realistic cyclonal circulation pattern which subdivides into two cells within the Greenland and Norwegian Seas, respectively.

Local surface salinity changes can also have severe effects. Figure 11a represents the Denmark Strait transport if the temperatures and salinities are restored to the Levitus winter values everywhere in the model, with a time constant increasing from 30 days at the surface to 250 days at 5000 m depth. (This 'robust diagnostic' technique is used to calculate the circulation resulting from a given tracer distribution and topography.) The transport over the Greenland–Iceland sill is almost zero, an indication that the Levitus data set is not consistent with the measured circulation. As is evident from other data sets, e.g. Dietrich (1969), this inconsistency can be attributed to a lack of freshwater runoff

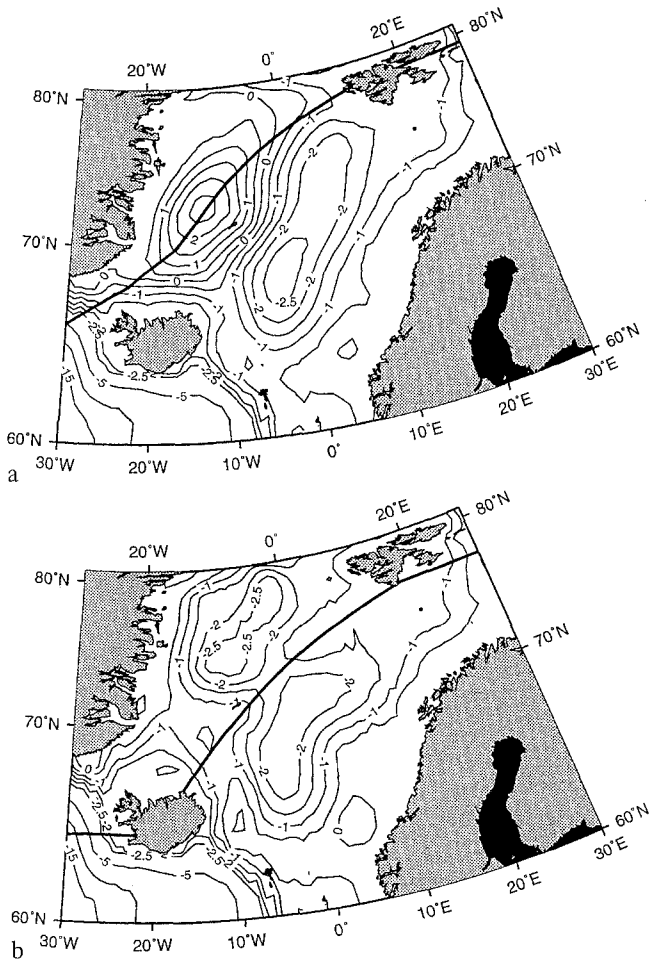

Fig. 10 **a, b** Effect of ice cover changes on the ocean circulation. **a** Narrow ice cover; **b** wider ice cover

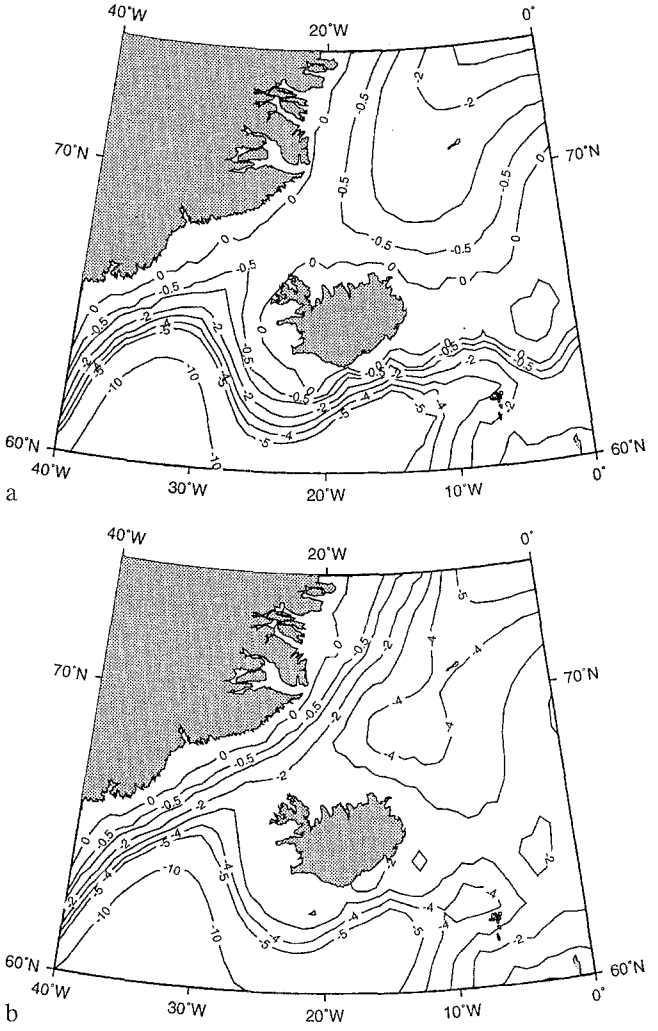

Fig. 11 **a, b** Effect of sea surface salinity on the transport of the East Greenland Current. **a** Levitus salinity; **b** artificial salinity (33‰)

from Greenland within the Levitus data sets. A salinitiy reduction of about 1–2‰ down to 33‰ along the coast of Greenland take this runoff into account and gives a more realistic outflow of approximately 2 Sv (Fig. 11b). This sensitivity is not confined to the overflow regions. Similar salinity changes or temperature variations of about 1–2° C can increase or decrease the basin-wide mass transports up to a factor of 10.

Owing to the uncertainties and spatial limitations of the available paleo-reconstructions, inconsistencies are an inseparable property of paleo-temperatures and paleo-salinities. SCINNA helps to filter out the consistent features and calculate the corresponding circulation.

Thus the results of the LGM experiment presented here are subject to further investigation, as the actual ice extent at 18000 years BP is not known exactly. Eventually, there might have been an ice-free region northeast of Iceland, which would slow down the cyclonal motion in the basin due to higher surface temperatures. Further on, the transports over the ridges could have been cut off completely by a suspected ice barrier between Greenland and Scotland.

The bottom circulation of the LGM and the M experiment will be compared along with the resulting sedimentation patterns modeled by SENNA and PATRINNA.

The four experiments (two with SENNA, two with PATRINNA) are initialized with the output data of SCINNA. These data sets contain the three-dimensional fields of temperature and salinity and the three-dimensional velocity field. For both time slices, M and LGM, the sediment properties – sediment sources, sinking velocity (0.05 cm s^{-1} = 43.2 m d^{-1}), density of sediment, grain size and sedimentological grain diameter, form factor of sediment particles and sediment porosity – are the same to simplify comparison of both experiments. In addition, the critical velocities for suspended load transport and bedload transport have been set to the same values in both instances.

The two experiments with PATRINNA, M and LGM, show the movement of particles parallel to the two-dimensional bottom layer (Fig. 12) within a period of 10 years. In both model runs 495 particles are started, which are equally distributed over the model area.

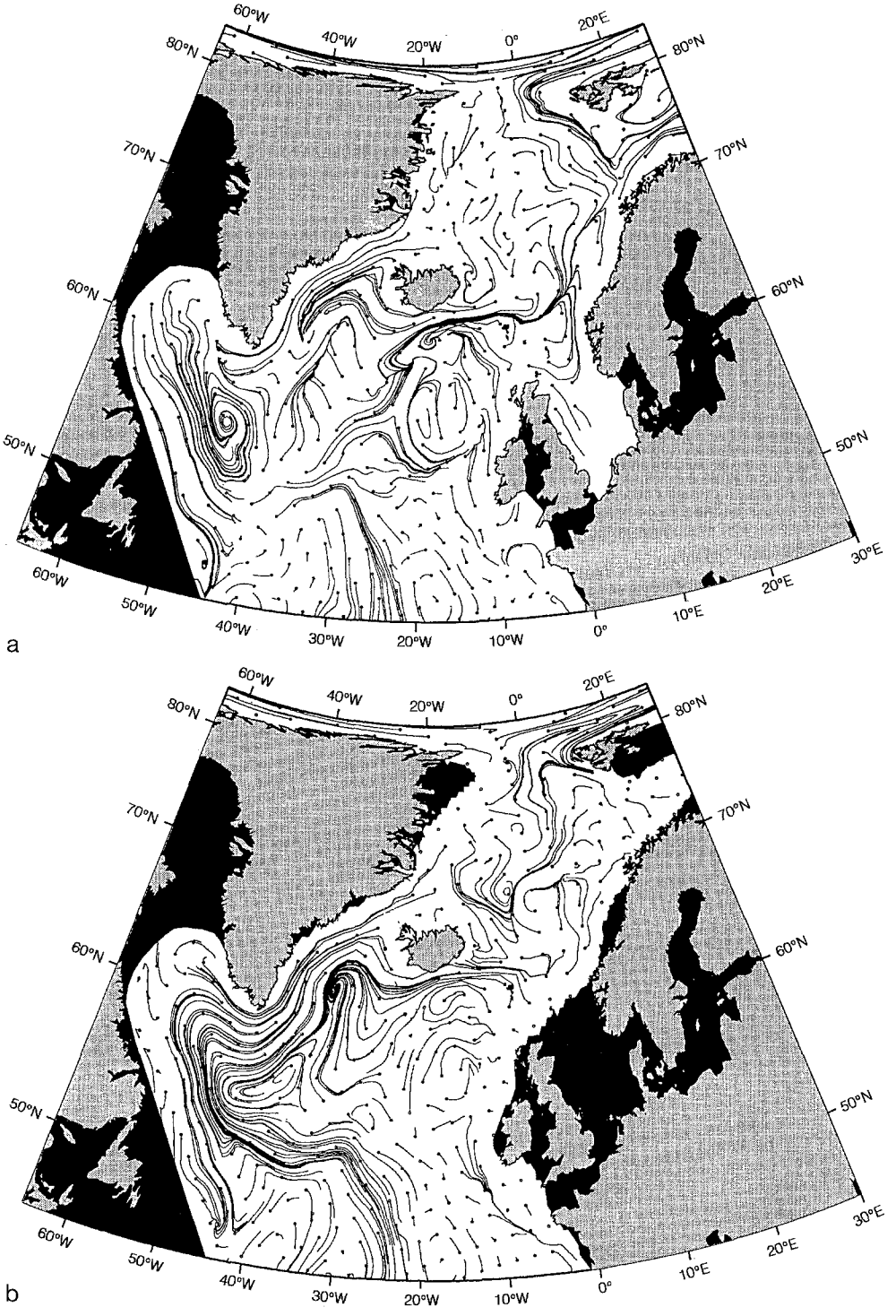

Fig. 12 **a** Modern particle traces in the bottom layer, 10 years transport. **b** LGM particle traces in the bottom layer, 10 years transport

In these experiments the magnitudes of the critical velocities for bedload and suspended transports are reduced to stay below the magnitudes of the horizontal velocities in the bottom layer. This simplifies working out the main sediment motions near the bottom. Previously published critical velocities (e.g. Hjulstrom 1939; Zanke 1978) cannot be used because they are developed for shallow water conditions rather than for deep sea regions. In shallow seas, near-bottom velocities are typically around 10 cm s^{-1}. In the deep basins of the models there are regions with only small values of about 1 cm s^{-1}. In all other parts in the deep sea they are less than 0.01 cm s^{-1}.

Figure 12a shows the particle traces induced by the main currents according to the actual state of knowledge, e.g. the Labrador, East Greenland, Irminger and Norwegian currents. These circulation and sediment transport patterns also appear during the last glacial maximum, but were in part laterally shifted and intensified (Fig. 12b).

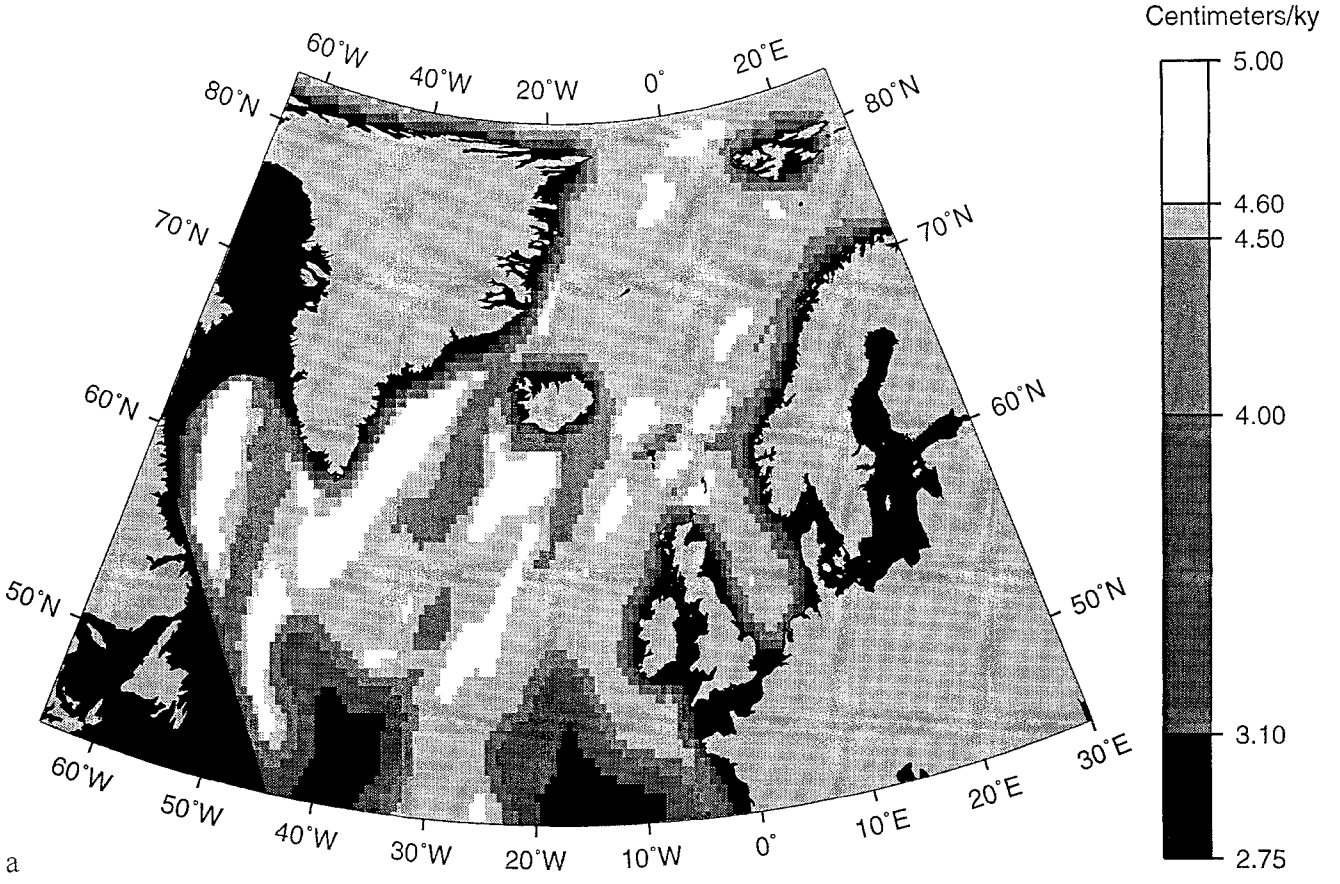

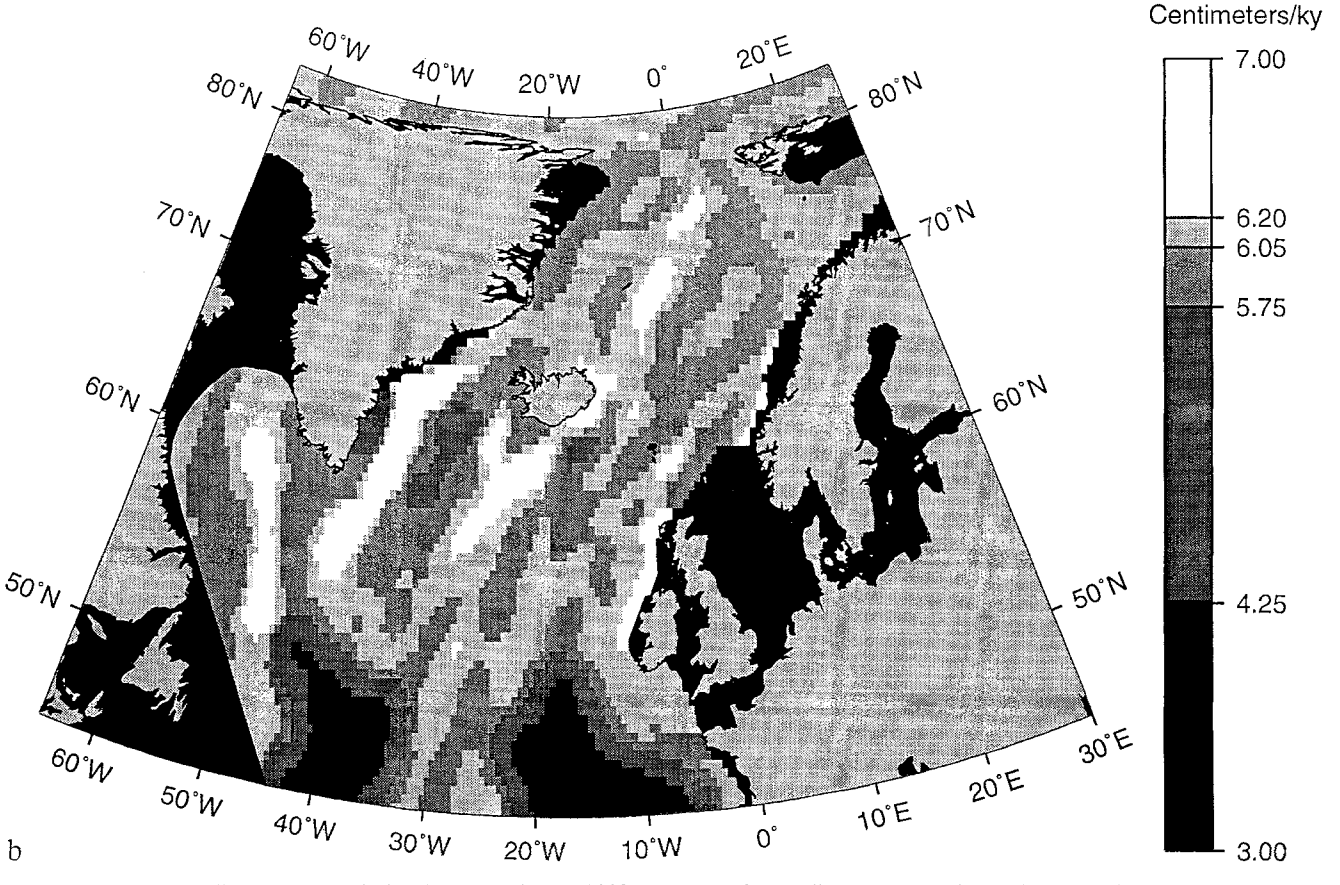

Fig. 13 **a** Modern sediment accumulation integrated over 2000 years. **b** LGM sediment accumulation integrated over 2000 years

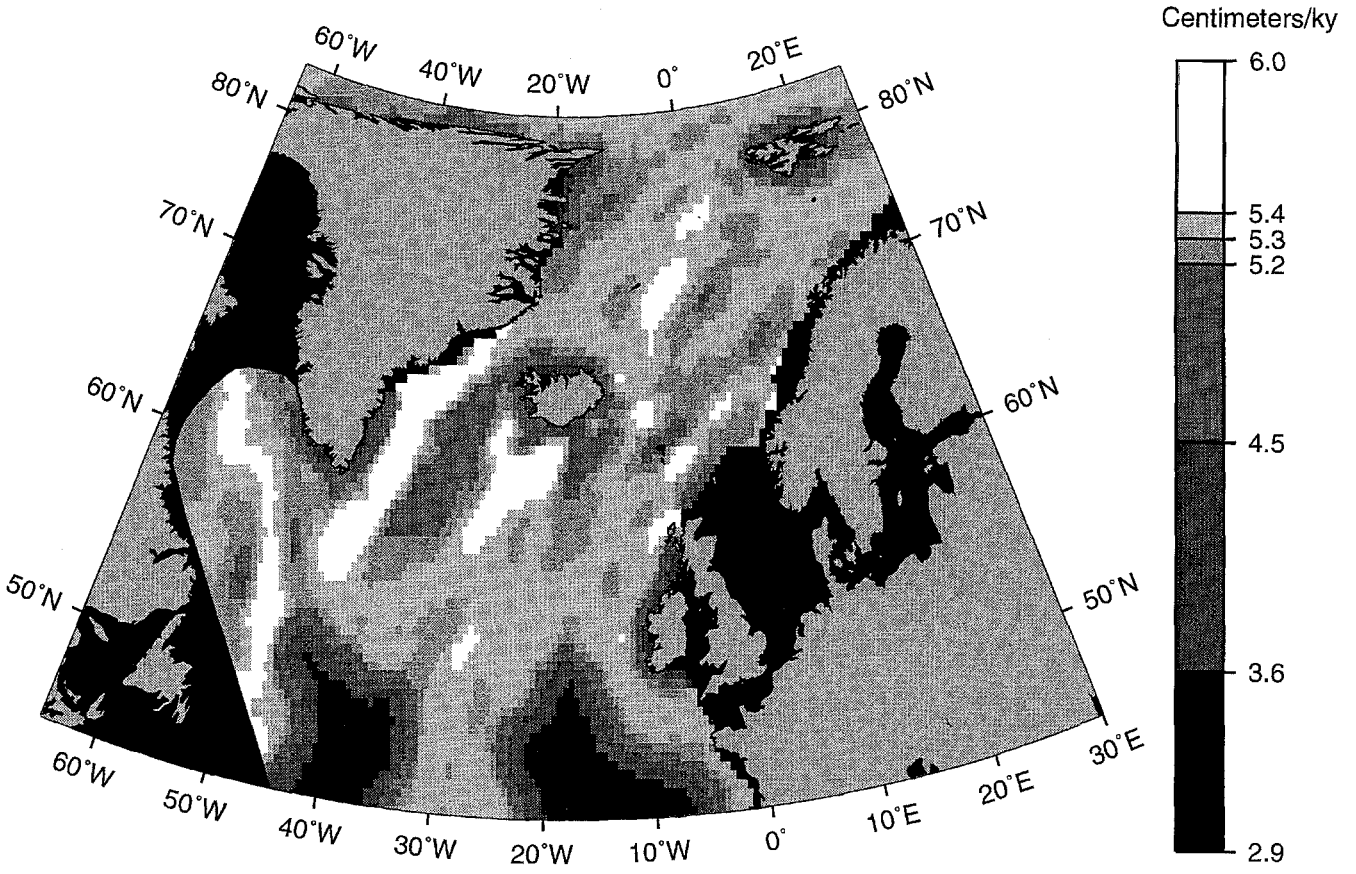

Fig. 14 Modern plus LGM sediment accumulation integrated over 2000 years

The two experiments with SENNA, M and LGM, show the amount of eroded, transported and finally deposited material (Fig. 13). Both model runs enclose a period of 2000 years. It is worth noting that both experiments use the same initialization for the sediment physics, but different initialization for the ocean physics (temperature, salinity and velocity), which are provided by the output of SCINNA's model runs.

Because the three-dimensional distribution of sediment sources and sinks has not yet been implemented completely in the numerical model, we assume for these first experiments that: (1) sediment input only occurs in the uppermost layer; (2) sediments are available on the seafloor; and (3) lateral input is not provides. The prescribed sediment flux is about 10^{-13} g cm^{-2} s^{-1} ($=0.0864$ mg m^{-2} d^{-1}). This value is lower than most published values (cf. Miller et al. 1977; Honjo 1990). In addition, the bedload and suspended load erosion rates, which depend on the bottom velocity, are reduced by a factor of 10^{-4} and 10^{-1}, respectively. These modifications have been introduced due to the fact that the most sensitive parameters in the model equations are, firstly, this erosion rate and, secondly, the critical velocities for bedload transport and supension load transport. In this way no small deep gaps in the bottom topography are produced in small areas with artificial high velocities.

Nevertheless, at this phase of development the model produces realistic patterns of sediment distribution (cf. McCave and Tucholke 1986). For example, if velocity and/or depth decrease in the direction of particle flow, the sediment is deposited. The same process takes place if there is an upward-directed bottom slope and when the two critical velocities increase.

The resulting sediment distribution patterns from SENNA show generally NE–SW directed sediment accumulations. Sedimentation rates are lower in the modern case than the LGM (up to 5 versus up to 7 cm per 1000 years). Most of the large sediment drifts in the NNA between the Greenland–Scotland Ridge and the Charlie Gibbs Fracture Zone can be identified as high accumulation areas. The sedimentation pattern of the modern state (Fig. 13a) is in part laterally shifted from the LGM state (Fig. 13b) due to the different oceanic circulation. Some areas yield continuous high sediment supply during both experiments, e.g. the Gloria Drift, Eirik Drift and Bjorn Drift, as can bee seen from Fig. 14 where the LGM and the modern accumulations have been added. The two southern regions of low sedimentation rate (darkly colored) are an artifact of the closed southern boundary. With the restoring technique used in SCINNA it is possible to simulate the missing inflow and outflow of sediment at this boundary to realistically prescribe the rest of the North Atlantic. This restoring can be performed by prescribing the sediment sources and sinks at all closed boundaries to take into account the terrigenous sediment input.

Conclusions

The NNA has been shown to be highly sensitive to small forcing changes. Small shifts of the ice-edge position can switch the circulation mode from cyclonal to anticyclonal; local variations of temperature or salinity by 1–2° or 1–2‰ may increase or decrease the overall transports by a factor of 10; the East Greenland Current can be turned on or off by changing the salinity by 1–2‰ along the coast of Greenland.

Based on these results, three-dimensional modeling of circulation changes during the last deglaciation cycle or melt water events is possible. The available data, however, are physically inconsistent to some extent. Thus they cannot be used to initialize and force models directly without further preparation.

Even the realistic modeling of the modern situation depends on a critical valuation of the measured data, but this does not pose unsolvable problems as there are enough available measurements. The real problem arises with the paleo-reconstructions due to their limitations in both spatial coverage and accuracy. The error estimates for paleo-temperatures and paleo-salinities are as large as or even larger than the variations discussed here. These errors can in fact cause purely artificial model results. Thus our aim is not to model past time slices in detail, but rather to reconstruct schematic and physically consistent distributions of temperature, salinity and ice, together with the respective circulation patterns.

As sediments in an oceanic basin develop together with ocean currents, a suitable modeling approach must take into account this strong dependence by coupling the processes of erosion, transport and deposition of sediments to the oceanic circulation pattern. In this way, our approach intends to base the sedimentation processes modeled by SENNA and PATRINNA on topography, temperatures, salinities and current velocities of the NNA calculated by SCINNA.

From our model experiments we have clear evidence that: (1) modeled and observed modern oceanic circulation and sedimentation show similar distribution patterns; (2) the three models and their coupling give reliable results for the modern case, and therefore this approach can be used for modeling the geological past; and (3) the general sedimentation patterns changed in time in accordance with the changes in the NNA circulation due to climatic changes, if we compare the LGM and modern cases.

Acknowledgements This work was supported by Deutsche Forschungsgemeinschaft, Special Research Project 313. We thank M. Sarnthein, M. Weinelt and D. Seidov for data, discussions and comments. The paper benefited from comments by K. Herterich and an anonymous reviewer.

References

Aukrust T, Oberhuber JM. Modelling of the Greenland, Iceland and Norwegian Seas with a coupled sea ice–mixed layer–isopycnal ocean model. J Geophy Res, in press

Bitzer K, Pflug R (1990) DEPOD: a three-dimensional model for simulating clastic sedimentation and isostatic compensation in sedimentary basins. In: Cross TA (ed) Quantitative Dynamics Stratigraphy. Prentice Hall, Englewood Cliffs, pp 335–348

Broecker W, Peng T-H (1982) Tracers in the Sea. Eldigio Press, Palisades, 689 pp

Bryan K (1969) A numerical method for the studys of the circulation of the world ocean. J Comp Phys 4:347–376

CLIMAP Project Members (1981) Seasonal Reconstructions of the Earth's Surface at the Last Glacial Maximum. GSA Map Chart Ser MC-36. Geological Society of America, Boulder

Cox MD (1984) A primitive equation, 3-dimensional model of the ocean. GFDL Ocean Group Tech Rep No 1. Geophysical Fluid Dynamics Laboratory / NOAA, Princeton University, 104 pp

Dietrich G (1969) Atlas of the Hydrography of the Northern North Atlantic. Conseil International pour l'Exploration de la Mer, Service Hydrographique, Charlottenlund Slot

Duplessy J-C, Labeyrie L, Juillet-Leclerc A, Maitre F, Dupart J, Sarnthein M (1991) Surface salinity reconstruction of the North Atlantic during the Last Glacial Maximum. Oceanol Acta 14:311–324

Ericksen M-C, Masson DS, Slingerland R, Swetland DW (1989) Numerical Simulation of Circulation and Sediment Transport in the Late Devonian Catskill Sea. In: Quantitative Dynamics Stratygraphy; Cross TA (ed), Prenctice Hall, Englewood Cliffs, pp 293–305

Gibbs RJ (1985) Settling velocity, diameter, and density for flocs of illite, kaolinite, and montmorillonite. J Sedim Petrol 55:65–68

Hellerman S, Rosenstein M (1983) Normal monthly wind stress over the world ocean with error estimates. J Phys Oceanogr 13:1093–1104

Hjulstrom F (1939) Transportation of detritus by moving water. In: Trask PD (ed) Recent Marine Sediments. American Association of Petroleum Geologists, Tulsa, pp 5–41

Honjo S (1990) Particle fluxes and modern sedimentation in the polar oceans. In: Smith WO (ed) Polar Oceanography, Part B, Academic Press, Inc., San Diego, New York, Boston, London, Sydney, Tokyo, Toronto, pp 687–739

Kendall CGStC, Moore P, Strobel J, Cannon R, Perlmutter M, Bezdek J, Biswas G. Simulation of the Sedimentary Fill of Basins; Kansas Geological Survey Bulletin, Vol 233, pp 9–30

Krohn J (1975) Ein mathematisches Modell des großräumigen gezeitenbedingten Sedimenttransports mit Anwendung auf die Nordsee. Master Thesis, Institut für Meereskunde, Hamburg

Lee Y-H, Harbaugh JW (1992) Stanford's SEDSIM Project. Dynamic three-dimensional simulation of geologic processes that affect clastic sediments. In: Pflug R, Harbaugh JW (eds) Computer Graphics in Geology. Lecture Notes Earth Sci 41. Springer, Berlin, Heidelberg, New York, pp 113–127

Legutke S (1991) Numerical experiments relating to the Great Salinity Anomaly of the seventies in the Greenland and Norwegian Seas. Progr Oceanogr 27:341–363

Levitus S (1982) Climatological Atlas of the World Ocean. NOAA Prof Pap 13. US Government Printing Office, Washington, 173 pp

McCave IN (1984) Erosion, transport and deposition of fine-grained marine sediments. In: Stow DA, Piper DJ (eds) Fine-grained Sediments: Deep-water Processes and Facies. Geological Society/Blackwell Scientific, Oxford pp 35–69

McCave IN, Gross TF (1991) In-situ measurements of particle settling velocity in deep sea. Mar Geol 99:403–411

McCave IN, Tucholke BE (1986) Deep current controlled sedimentation in the western North Atlantic. In: Vogt PR, Tucholke BE (eds) The Geology of North America, Vol M. Geological Society of America, Boulder, pp 451–468

Mesinger F, Arakawa A (1976) Numerical Methods Used in Atmospheric Models. GARP Publ Ser 17:64 pp

Miller MC, McCave IN, Komar PD (1977) Threshold of sediment motion under unidirectional currents. Sedimentology 24:507–528

Pacanowski R, Dixon K, Rosati A (1991, 1993) The G.F.D.L. Molecular Ocean Model Users Guide. GFDL Ocean Group Tech Rep 2
Pflaumann U, Duprat J, Pujol C, Labeyrie D. SIMMAX, a transfer technique to deduce Atlantic sea surface temperatures from planktonic foraminifera – the EPOCH approach. Paleoceanography, submitted
Puls W (1981) Numerical simulation of bedform mechanics. Mitteilungen Inst Meereskunde Univ Hamburg 24:1–147
Sarnthein M, Jansen E, Arnold M, Duplessy J-C, Erlenkeuser H, Flatoy A, Veum T, Vogelsang E, Weinelt MS (1992) A time-slice reconstruction of meltwater anomalies at termination I in the North Atlantic between 50 and 80 N. In: Bard E, Broecker WS (edS) The Last Deglaciation: Absolute and Radiocarbon Chronologies. NATO ASI Ser 12. Springer, Berlin, Heidelberg, New York, pp 183–200
Sarnthein M, Winn K, Jung S, Duplessy J-C, Labeyrie L, Erlenkeuser H, Ganssen G (1994) Changes in East Atlantic deep-water circulation over the last 30000 years: Eight time slice reconstructions. Paleoceanography, Vol 9, No 2, pp 209–267
Seidov D, Sarnthein M, Stattegger K (1994) Toward a better understanding of the meltwater event near 13.6 ky bp – a numerical modelling approach, in preparation
Stevens DP (1991) A numerical ocean circulation model of the Norwegian and Greenland Sea. Progr Oceanogr 27:365–402
Sündermann J, Klöcker R (1983) Sediment transport modelling with applications to the North Sea. In: Sündermann J, Lenz W (eds) North Sea Dynamics. Springer, Berlin, Heidelberg, New York, pp 453–471
Syvitski JPM, Daughney S (1992) Delta 2: Delta Progadation and Basin Filling, Computer & Geosciences, Vol 18, No 7, pp 839–897
Tetzlaff DN, Harbaugh JW (1989) Simulating Clastic Sedimentation. Van Nostrand Reinhold, New York, 202 pp
Zanke U (1977) Berechnung von Sinkgeschwindigkeiten von Sedimenten. Mitteilungen Franzius Inst Wasserbau Küsteningenieurswesen Tech Univ Hannover 46:230–245
Zanke U (1978) Zusammenhänge zwischen Strömung und Sedimenttransport; Teil 1: Berechnung des Sedimenttransportes – allgemeiner Fall. Mitteilungen Franzius Inst Wasserbau Küsteningenieurswesen Tech Univ Hannover 47:214–345

Appendix: symbols and definitions

Symbols

a	Earth's radius
g	Gravitational acceleration
Ω, $f=2\Omega \sin \phi$	Earth's angular velocity, Coriolis parameter
λ, ϕ, z	Longitude, latitude and depth
$\Delta\lambda$, $\Delta\phi$, Δz	Zonal, meridional and vertical grid spacing
H	Water depth
Δt	Time step
u, v, w	Zonal, meridional and vertical components of velocity
Ψ	Stream function (vertically integrated mass transport)
u_{bot}, v_{bot}	Reduced zonal and meridional bottom velocity components
u_{Scrit}, v_{Scrit}	Critical velocities for suspended load transport
u_{Bcrit}, v_{Bcrit}	Critical velocities for bedload transport
w_{sink}	Sinking velocity of sediment particles
T, S, C	Temperature, Salinity and Sediment concentration
ϱ, ϱ_0	Density and mean density of sea water
ν	Kinematic viscosity of sea water
gs, D^*	Grain size and sedimentological grain diameter
FF	Form factor of sediment particles
$\varrho_{sediment}$	Sediment density
γ	Sediment porosity
p, p_{surf}	Pressure, surface pressure
τ^λ, τ^ϕ	Zonal and meridional wind stress
τ_B^λ, τ_B^ϕ	Zonal and meridional bottom friction
A_{MH}, A_{MV}	Horizontal and vertical mixing coefficient for momentum
A_{TH}, A_{TV}	Horizontal and vertical mixing coefficient for tracers

Definitions

μ being used as placeholder for T, S, C, u or v

μ_t	Time derivative
μ_λ, μ_ϕ, μ_z	Zonal, meridional and vertical derivatives
μ_n	Derivative normal to boundary
$\mathscr{L}\mu = \frac{\sec\phi}{a}[(u\mu)_\lambda + (v\mu\cos\phi)_\phi] + (w\mu)_z$	Three-dimensional advection operator
$\mathscr{L}_H\mu = \frac{\sec\phi}{a}[(u\mu)_\lambda + (v\mu\cos 1\ \phi)_\phi]$	Two dimensional advection operator
$\nabla^2\mu = 1\sec^2\phi\mu_{\lambda\lambda} + \sec\phi(\mu_\phi\cos\phi)_\phi$	Two-dimensional Laplacian operator
$\mathscr{D}^u = (A_{MV}u_z)_z + \frac{A_{MH}}{a^2}[\nabla^2 u + (1-\tan^2\phi)\ u - 2\sin\phi\sec^2\phi v_\lambda]$	u turbulent mixing operator
$\mathscr{D}^v = (A_{MV}v_z)_z + \frac{A_{MH}}{a^2}[\nabla^2 v + (1-\tan^2\phi)\ v + 2\sin\phi\sec^2\phi u_\lambda]$	v turbulent mixing operator
$\mathscr{D} = (A_{TV}\mu_z)_z + \frac{A_{TH}}{a^2}\nabla^2\mu$	Three-dimensional tracer diffusion operator
$\mathscr{D}_H = \frac{A_{TH}}{a^2}\nabla^2\mu$	Two-dimensional tracer diffusion operator
$\mathscr{P}_\lambda = \frac{\sec\phi}{a\varrho_0}p_\lambda$, $\mathscr{P}_\phi = \frac{1}{a\varrho_0}p_\phi$	Zonal and meridional pressure forces
$\mathscr{C}^\mu$	T and S convective adjustment
$\mathscr{R}^\mu$	T and S restoring
$\mathscr{S}$	Sediment sources